magnetochemistry

MDPI

Article

Modulating the Slow Relaxation Dynamics of Binuclear Dysprosium(III) Complexes through Coordination Geometry

Amit Kumar Mondal, Vijay Singh Parmar and Sanjit Konar *

Department of Chemistry, Indian Institute of Science Education and Research Bhopal, Bhopal 462066, MP, India; amondal@iiserb.ac.in (A.K.M.); vsparmar@iiserb.ac.in (V.S.P.)
* Correspondence: skonar@iiserb.ac.in; Tel.: +91-755-6692339

Academic Editor: Floriana Tuna
Received: 30 August 2016; Accepted: 13 September 2016; Published: 21 September 2016

Abstract: A class of two dinuclear dysprosium based complexes **1** and **2** were synthesized by employing salicyloylhydrazone derived pentadentate ligand (L). Structural analysis reveals that in complex **1**, two Dy^{III} centers are in muffin (C_s) coordination geometry while in **2**, one Dy^{III} center is in bicapped square antiprism (D_{4d}) and other one is in triangular dodecahedron (D_{2d}) coordination geometry. AC magnetic susceptibility measurements disclose that complexes **1** and **2** exhibit single-molecule magnet (SMM) behavior, with effective energy barrier of 36.4 and 9.7 K, respectively. The overall studies reveal that small differences in the coordination environment around the Dy^{III} centers played a significant role in the difference in relaxation dynamics of the complexes. In order to elucidate the role of intermolecular interactions between nearby Dy^{III} centers in the magnetic relaxation behavior, a diamagnetic isostructural Y^{III} analog (**3**) was synthesized and magnetic behavior was examined.

Keywords: dysprosium; slow magnetic relaxation; coordination environment

1. Introduction

In recent years, single molecule magnets (SMMs), a unique class of nano-dimensional magnetic materials, have attracted significant research interest. SMMs have potential applications in a variety of fields, including high-density data storage devices, quantum computing, and molecular spintronics [1]. The importance of SMMs is that, even in the absence of an external magnetic field, they can preserve the magnetization for long period of time at low temperatures. After an extensive research on 3d metal complexes in the last decade [2–4], a rapid development of Ln based SMMs has been observed in recent years [5–9]. Compared to 3d metals, Ln based SMMs are mostly investigated owing to the fact that the Ln^{III} ions such as Dy^{III}, Tb^{III}, Er^{III}, and Ho^{III} have huge and unquenched orbital angular momentum [10–12] which causes substantial magnetic anisotropy. The major approach for the construction of such systems is to choose a ligand field (LF) which could offer an axial crystal field acting on the Ln^{III} ion and stabilize the M_J states with a large absolute value of the total angular momentum projection $|M_J|$, therefore realizing a magnetization easy axis. Outstanding Ln based SMMs include Tb^{III}/Dy^{III}-phthalocyanin (Pc) double-decker complexes [13] and sandwiched Er^{III} complexes with polyoxometallate based ligands [14]. Dinuclear Ln SMMs represent the simplest molecular units which permit the study of magnetic interactions between two spin carriers. If a dinuclear SMM can be designed in a controllable manner, it can be possible to construct larger molecules via a bottom up molecular approach and make SMMs with higher blocking temperatures. Herein two dinuclear complexes $[Dy_2(L)_2(MeOH)_2(NO_3)_2]\cdot(MeOH)\cdot(CH_2Cl_2)$ (**1**) and $[Dy_2(L)_3(H_2O)\cdot(MeOH)]\cdot(MeOH)_4\cdot(H_2O)$ (**2**) are

reported, which are obtained from the reaction of a pentadentate organic ligand L with $Dy(NO_3)_3$ and $DyCl_3$, respectively (*L* = 2,6-bis(1-salicyloylhydrazonoethyl) pyridine; Figure S1).

As the overall electronic structure of a Dy^{III} ion is very sensitive to its coordination environment, minor changes in the ligand systems can significantly affect the magnetic properties of the complexes [15–17]. Most of the reports on Ln-based SMMs concentrated mainly on either changing the Ln ion keeping the ligand system constant [18–20] or changing the ligand but keeping the coordination environment around the Ln ion unchanged [8]. Only few studies are known where modification in the ligand system was done to tune the relaxation behavior in the complexes [21–26]. In this paper, differences in slow relaxation of the magnetization behavior were explored in two Dy^{III} dinuclear complexes, where minor changes in the coordination environment around the Dy^{III} ions disturbed the local symmetry.

2. Results and Discussion

Single-crystal X-ray analysis showed that both the complexes crystallize in the triclinic *P*-1 space groups (Table 1). The molecular structures of the complexes are shown in Figure 1. For complex **1**, both Dy^{III} centers contain similar DyN_3O_6 cores, surrounded by the ligand, one coordinated nitrate anion, one methanol molecule and one phenoxide oxygen atom of another ligand, whereas for complex **2**, both Dy^{III} centers contain different DyN_6O_4 and DyN_3O_5 cores. Two interlocked pentachelating ligands make up the coordination sphere of one Dy^{III} center, while other one is surrounded by the ligand, one coordinated methanol molecule, one water molecule and one phenoxide oxygen atom of another ligand. In both complexes, ligand coordinates via the pyridyl nitrogen, both hydrazone nitrogen and both carbonyl oxygen atoms. The C–O bond lengths in **1** and **2** (Tables S1 and S2) are all in good agreement with their assignment as carbonyls (1.225(5)–1.265(6) Å) rather than alkoxides [27]. The structural differences between **1** and **2** were deeply investigated since the coordination environment around the Dy^{III} ion has a dramatic influence on the magnetic properties of the resulting complexes [28]. Systematic analysis of the coordination geometries around the Dy^{III} centers using SHAPE 2.1 [29] reveals that the nine-coordinated Dy^{III} centers of complex **1** adopt geometries that are best described as muffin (minimum CShM values of 2.565), whereas for complex **2**, the ten- and eight-coordinated Dy^{III} centers adopt bicapped square antiprism and triangular dodecahedron coordination geometries, respectively (minimum CShM values of 3.125 and 3.548 were obtained) (Table S3).

In complex **1**, all the hydrogen atoms from the coordinated methanol molecules are involved in intermolecular hydrogen bonding (Table S4) with the phenoxy oxygen atoms and these interactions support the formation of a supramolecular two dimensional arrangement (Figures S2 and S3). In complex **2**, all the hydrogen atoms of coordinated methanol and water molecules are involved in intermolecular hydrogen bonding (Table S5) with the phenoxy oxygen atoms and lattice methanol molecules resulting in the formation of a supramolecular two dimensional arrangement (Figures S4 and S5). In addition to the H-bonding interactions, strong CH$\cdots\pi$ interactions are also noticed with CH to centroid distances of 3.595(4) Å and 3.508(6) Å for **1** and **2**, respectively.

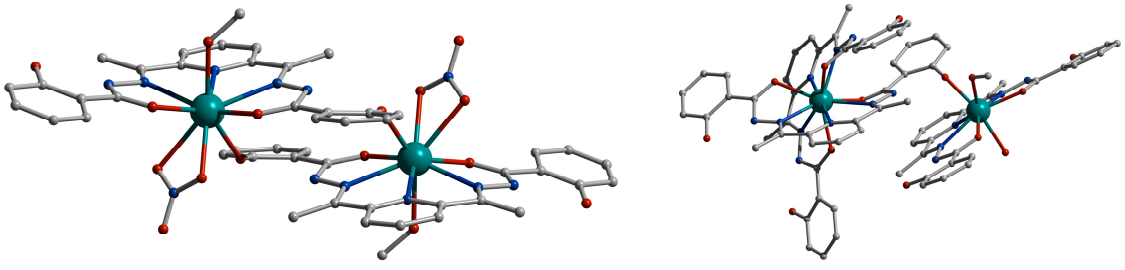

(**a**) (**b**)

Figure 1. *Cont.*

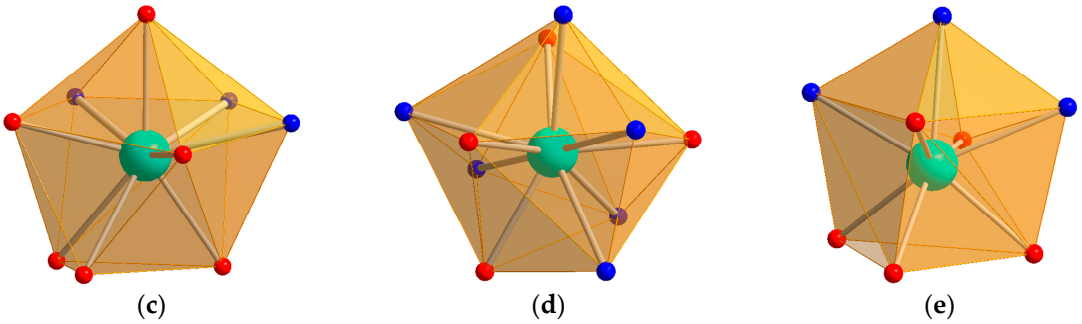

(**c**) (**d**) (**e**)

Figure 1. View of the molecular structures of: complex **1** (**a**); and complex **2** (**b**). Polyhedral view of: nine- (**c**); ten- (**d**); and eight- (**e**) coordinated geometries of Dy^{III} centers found in complexes **1** and **2**.

Table 1. X-ray Crystallographic Data and Refinement Parameters for complexes **1** and **2**.

	1	**2**
Formula	$C_{52}H_{54}Cl_4Dy_2N_{12}O_{18}$	$C_{74}H_{76}Dy_2N_{15}O_{19}$
M_w (g·mol^{-1})	1601.87	1804.50
Crystal size (mm)	0.45 × 0.18 × 0.16	0.43 × 0.15 × 0.10
Crystal system	Triclinic	Triclinic
Space group	*P*-1	*P*-1
T (K)	296(2)	151(2)
a (Å)	10.868(3)	12.7428(8)
b (Å)	10.872(3)	16.2939(9)
c (Å)	12.955(3)	19.1396(11)
α (°)	84.323(14)	89.6900(18)
β (°)	85.574(13)	85.6640(18)
γ (°)	76.415(13)	75.657(2)
V (Å^3)	1478.3(7)	3838.7(4)
Z	1	2
ρ_{calcd} (g·cm^{-3})	1.799	1.561
μ (MoKα) (mm^{-1})	2.771	2.012
F(000)	794.0	1818.0
T_{max}, T_{min}	0.652, 0.545	0.828, 0.723
h, *k*, *l* range	$-14 \le h \le 13$, $-14 \le k \le 14$, $-16 \le l \le 16$	$-15 \le h \le 15$, $-20 \le k \le 20$, $-23 \le l \le 23$
Collected reflections	6645	15689
Independent reflections	5667	9904
Goodness-of-fit (GOF) on F^2	1.038	1.456
*R*1, *wR*2 ($I > 2\sigma I$)	0.0444, 0.1163	0.0494, 0.0794
*R*1, *wR*2 (all data)	0.0518, 0.1229	0.0887, 0.0842
CCDC Number	1482439	1482440

$R1 = \Sigma||Fo| - |Fc||/\Sigma|Fo|$ and $wR2 = |\Sigma w(|Fo|^2 - |Fc|^2)|/\Sigma|w(Fo)^2|^{1/2}$.

The purity of the as-synthesized products was confirmed by the good agreements of the bulk phase powder X-ray diffraction patterns with the simulated one (Figure S6). Elemental composition of **1** and **2** were confirmed by the elemental analysis, which matches well with the calculated values. The IR spectra of complexes **1** and **2** show bands at ~3434 cm^{-1}, 1640 cm^{-1}, 1583 cm^{-1} and 1018 cm^{-1}, which can be assigned to ν(phenolic OH), ν(C=N), pyridine ring stretching vibrations and ν(N–N), respectively. The bands at 1435 cm^{-1}, 1304 cm^{-1} and 1030 cm^{-1} clearly identify the presence of coordinated nitrate in complex **1**. In the IR spectrum of **2**, the bands at ca. 3221 and 819 cm^{-1} are characteristic of coordinated water molecule in complex **2**.

The variable-temperature DC magnetic susceptibility measurements were performed under an applied field of 1000 Oe and in the range of 1.8–300 K. The room temperature experimentally obtained $\chi_M T$ values for complexes **1** and **2** are 28.4 and 28.3 cm^3·K·mol^{-1}, respectively (Figure 2 and Figure S7), which are consistent with the theoretical value of 28.34 cm^3·K·mol^{-1} for two isolated Dy^{III} ions [15]. On lowering the temperature from 300 K, the $\chi_M T$ value decreases gradually due to the single ion crystal-field effects. This result is further prominent below 70 K, where it reaches value of

10.9 and 10.7 $cm^3 \cdot K \cdot mol^{-1}$ for **1** and **2**, respectively, at 2 K. The observation reveals the continuous depopulation of the excited Stark sublevels of the Dy^{III} ions [30].

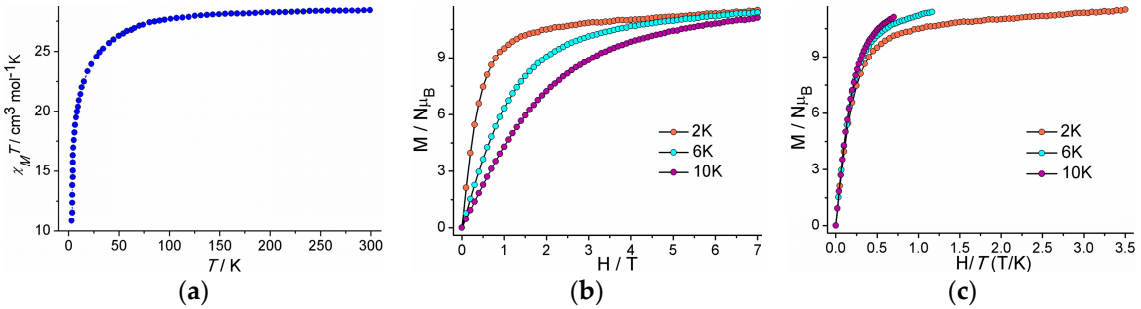

Figure 2. (**a**) $\chi_M T$ vs. T plot measured at 0.1 T for complex **1**; and $M/N\mu_B$ vs. H (**b**); and $M/N\mu_B$ vs. H/T plots (**c**) in the field range of 0–7 T and temperature range of 2–10 K for complex **1**.

The reduced magnetization data ($M/N\mu_B$ vs. H) of the complexes were collected at 2, 6 and 10 K. For **1** and **2**, with increase in field $M/N\mu_B$ values increase sharply and attained the values of 11.5 and 11.2 $N\mu_B$ respectively (Figure 2 and Figure S7), which are in good agreement with the theoretical value for Dy^{III}-based SMMs [8]. As shown in Figure 2 and Figure S7, all isotherm magnetization curves do not merge, which confirms the presence of large magnetic anisotropy in the complexes [10].

To probe spin dynamics in **1** and **2**, ac magnetic susceptibility measurements were carried out at 3.5 Oe ac field and varying the temperature from 1.8–10 K under zero dc field. Complexes **1** and **2** show temperature (Figure 3 and Figure S8) and frequency dependency (Figures S9 and S10) of out of phase (χ_M'') ac susceptibilities. The phenomenon indicates the single-molecule magnet (SMM) like behavior in the complexes [6]. Moreover, the Cole–Cole plots [31,32] (Figure 3 and Figure S11) were generated from the frequency-dependent ac susceptibility data. The fit of the χ_M'' vs. χ_M' data using the generalized Debye model [31,32] produced the values of α within the ranges 0.05–0.27 (**1**) and 0.08–0.32 (**2**), signifying the narrow distribution of the relaxation time. Effective energy barrier (U_{eff}) and relaxation time (τ_0) were calculated from the Arrhenius Equation (1) [33–35]:

$$\ln(1/\tau) = \ln(1/\tau_0) - U_{eff}/kT \quad (1)$$

where k = Boltzmann constant, and $1/\tau_0$ = pre-exponential factor. The linear fit to high temperature data gave values of U_{eff} = 36.4 K and $\tau_0 = 3.3 \times 10^{-6}$ s for **1** (Figure 3). However, the out-of-phase signals (χ_M'') for complex **2** do not show the peak maxima in the mentioned temperature range. Therefore, Debye model and Equation (2) were used to calculate energy barrier and relaxation time [36]

$$\ln(\chi''/\chi') = \ln(\omega\tau_0) + U_{eff}/kT \quad (2)$$

From the best fitting, the value of energy barrier and relaxation time were calculated as U_{eff} = 9.7 K and $\tau_0 = 1.4 \times 10^{-6}$ s, respectively (Figure S11), and found to be in good agreement with the expected value of 10^{-6}–10^{-11} for a SMM [37–39].

In order to explore the consequence of inter- and intramolecular exchange interactions on the magnetic behavior, the influence of magnetic dilution on relaxation of the magnetization was studied. To gain more in sight we synthesized the diamagnetic dinuclear Y^{III} analog (**3**) (see ESI for experimental and X-ray details, Figure S12 and Table S6) and then prepared the doped sample in which the Dy^{III} complex (**1**) was magnetically diluted with the Y^{III} complex in a 5:95 ratio. AC susceptibility measurements were performed on a polycrystalline sample of the diluted complex. No major difference was found in the energy barrier of the diluted sample compared to the undiluted one (Figure S13). Therefore, it can be concluded that the intermolecular forces and dipolar interactions are insignificant in this case.

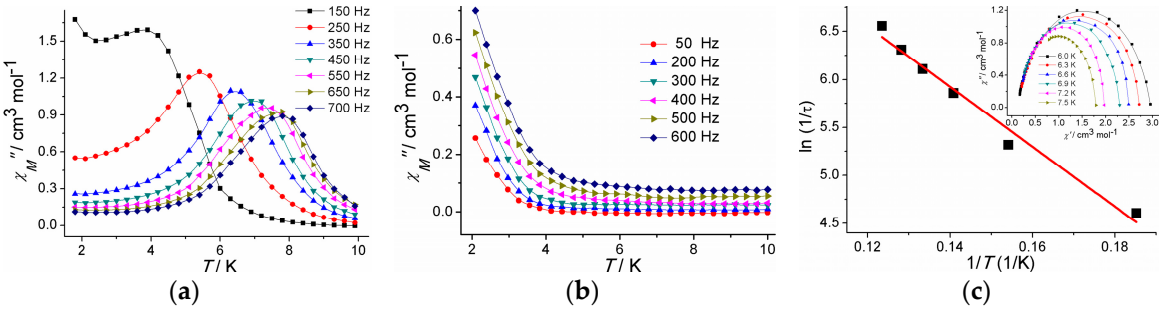

Figure 3. Temperature dependence of the out-of-phase (χ_M'') AC magnetic susceptibility plots for: complex **1** (**a**); and complex **2** (**b**); Illustration of (**c**) $\ln(1/\tau)$ vs. $1/T$ plots for **1** (red lines represents the best fit of the Arrhenius relationship). Cole–Cole plots for **1** are shown in the inset.

From comparative point of view, even though **1** and **2** contain two Dy^{III} centers, their relaxation dynamic behaviors are considerably different. The difference was attributed to the slight changes in the coordination environments around the Dy^{III} centers [19,27,40–42]. This is due to the nature and symmetry of crystal field which controls anisotropy and effects on overall effective energy barrier [43–47]. As can be seen, in complex **1**, two Dy^{III} centers are in muffin (C_s) geometry, while in **2**, one Dy^{III} center is in bicapped square antiprism (D_{4d}) and other one is in triangular dodecahedron (D_{2d}) geometry. Hence, the observed difference in magnetic behaviors of **1** and **2** was mostly because of the different coordination environments around the Dy^{III} centers, which affects the nature of easy axes [43].

3. Materials and Methods

All chemicals were of reagent grade and used without further purification. The elemental analyses were carried out on an Elementar Microvario (Mumbai, India) Cube Elemental Analyzer. FT-IR spectra (4000–400 cm^{-1}) were recorded on KBr pellets using a Perkin-Elmer (Mumbai, India) Spectrum BX spectrometer. Powder X-ray diffraction (PXRD) data were collected on a PANalytical EMPYREAN (Mumbai, India) instrument using Cu-Kα radiation. Magnetic measurements were performed using a SQUID VSM magnetometer (Quantum Design, Mumbai, India). The measured values were corrected for the experimentally measured contribution of the sample holder, while the derived susceptibilities were corrected for the diamagnetism of the samples, estimated from Pascal's tables [48].

Ligand was prepared by a simple hydrazine condensation reaction of one equivalent 2,6-diacetylpyridine with two equivalents of 2-salicyloylhydrazide in methanol according to an earlier reported procedure [49].

Synthesis of $[Dy_2(L)_2(MeOH)_2(NO_3)_2]$ (MeOH) (CH_2Cl_2) (**1**). L (43 mg, 0.1 mmol) was dissolved in CH_2Cl_2 (5 mL) and the solution was warmed to 45 °C. $LiOH{\cdot}H_2O$ (4.0 mg, 0.1 mmol) was added to the reaction mixture to deprotonate the ligand. Then, $Dy(NO_3)_3{\cdot}5H_2O$ (43 mg, 0.1 mmol) dissolved in MeOH (5 mL) and added to the above ligand solution. The solution formed an intense yellow mixture and it was stirred for another 2 h. The solution was filtered off and the filtrate was left in open atmosphere for slow evaporation which gives large X-ray quality yellow crystals of $[Dy_2(L)_2(MeOH)_2(NO_3)_2]$ (MeOH) (CH_2Cl_2) (**1**) after 4 days. The crystals were separated and washed with cold water and Et_2O; yield (57%). Anal. Calcd for $C_{52}H_{54}Cl_4Dy_2N_{12}O_{18}$: C, 38.99; H, 3.40; N, 10.49%. Found: C, 39.09; H, 3.47; N, 10.41%. Selected IR data (KBr pellet, 4000–400 cm^{-1}) ν/cm^{-1}: 3434, 1640, 1580, 1435, 1304, 1030, 1018.

Synthesis of $[Dy_2(L)_3(H_2O)$ (MeOH)] $(MeOH)_4$ (H_2O) (**2**). L (65 mg, 0.15 mmol) was dissolved in CH_2Cl_2 (5 mL) and the solution was warmed to 45 °C. $LiOH{\cdot}H_2O$ (4.0 mg, 0.1 mmol) was added to the reaction mixture to deprotonate the ligand. Then, $DyCl_3{\cdot}6H_2O$ (38 mg, 0.1 mmol) dissolved in MeOH (5 mL) and added to the above ligand solution. The solution formed an intense yellow mixture and it was stirred for another 3 h. The solution was filtered off and the filtrate was left in open atmosphere for

slow evaporation which gives large X-ray quality yellow crystals of $[Dy_2(L)_3(H_2O)\ (MeOH)]\ (MeOH)_4\ (H_2O)$ (**2**) after 5 days. The crystals were separated and washed with cold water and Et_2O; yield (65%). Anal. Calcd for $C_{74}H_{80}Dy_2N_{15}O_{19}$: C, 49.15; H, 4.46; N, 11.62%. Found: C, 49.24; H, 4.34; N, 11.69%. Selected IR data (KBr pellet, 4000–400 cm^{-1}) ν/cm^{-1}: 3430, 3221, 1642, 1583, 1020, 819.

Intensity data were collected on a Brüker (Mumbai, India) APEX-II CCD diffractometer using a graphite monochromated Mo-Kα radiation (α = 0.71073 Å). Data collection was performed using ϕ and ω scan. Direct methods were used for the solution of crystals using SHELXTL followed by full matric least square refinements against F^2 [50]. The positions of the remaining non-hydrogen atoms were found by using difference Fourier synthesis and least square refinements. The exact crystal system, cell dimensions and orientation matrix were determined by the reported procedure followed by multi-scan absorption correction and Lorentx polarization. All H-atoms were calculated geometrically and refined using riding model. The non-hydrogen atoms were refined with anisotropic displacement parameters. SHELXL 97 [51], PLATON 99 [52] and WinGXsystemVer-1.64 [53] were used for the refinement and calculations. The details of collection of data and their refinement parameters are included in Table 1.

4. Conclusions

Two important dinuclear dysprosium based complexes have been synthesized and characterized. Both the complexes exhibit single-molecule magnet (SMM) like behavior. It has been observed that a minor difference in the coordination surroundings around the Dy^{III} center affected the relaxation dynamics of the complexes. Therefore, the overall studies propose the importance of the coordination environment around Dy^{III} centers in describing and distinguishing their magnetic properties. Further studies along similar lines are in progress.

Supplementary Materials: The following are available online at www.mdpi.com/2312-7481/2/3/35/s1. Coordination polyhedral, SHAPE analysis table, magnetic plots, PXRD, bond length and bond distances tables and hydrogen bonding tables.

Acknowledgments: A.K.M. thanks UGC for SRF fellowship. V.S.P. thanks IISER Bhopal for fellowship. S.K. thanks DAE BRNS, 37(2)/14/09/2015/BRNS, Government of India and IISER Bhopal for generous financial and infrastructural support.

Author Contributions: A.K.M. designed and performed the experiments; A.K.M. solved the crystal structures and analyzed the magnetic data; A.K.M. and V.S.P. wrote the paper; and S.K. supervised the overall work and organized the project.

Conflicts of Interest: The authors declare no conflict of interest.

References

1. Urdampilleta, M.; Klyatskaya, S.; Cleuziou, J.-P.; Ruben, M.; Wernsdorfer, W. Supramolecular spin valves. *Nat. Mater.* **2011**, *10*, 502–506. [CrossRef] [PubMed]
2. Brechin, E.K.; Boskovic, C.; Wernsdorfer, W.; Yoo, J.; Yamaguchi, A.; Saňudo, E.C.; Concolino, T.R.; Rheingold, A.L.; Ishimoto, H.; Hendrickson, D.N.; et al. Quantum Tunneling of Magnetization in a New $[Mn_{18}]^{2+}$ Single-Molecule Magnet with S = 13. *J. Am. Chem. Soc.* **2002**, *124*, 9710–9711. [CrossRef] [PubMed]
3. Boskovic, C.; Brechin, E.K.; Streib, W.E.; Folting, K.; Bollinger, J.C.; Hendrickson, D.N.; Christou, G. Single-Molecule Magnets: A New Family of Mn_{12} Clusters of Formula $[Mn_{12}O_8X_4(O_2CPh)_8L_6]$. *J. Am. Chem. Soc.* **2002**, *124*, 3725–3736. [CrossRef] [PubMed]
4. Manoli, M.; Johnstone, R.D.L.; Parsons, S.; Murrie, M.; Affronte, M.; Evangelisti, M.; Brechin, E.K.A. Ferromagnetic Mixed-Valent Mn Supertetrahedron: Towards Low-Temperature Magnetic Refrigeration with Molecular Clusters. *Angew. Chem. Int. Ed.* **2007**, *46*, 4456–4460. [CrossRef] [PubMed]
5. Aromí, G.; Aguilá, D.; Gamez, P.; Luis, F.; Roubeau, O. Design of magnetic coordination complexes for quantum computing. *Chem. Soc. Rev.* **2012**, *41*, 537–546. [CrossRef] [PubMed]
6. Woodruff, D.N.; Winpenny, R.E.P.; Layfield, R.A. Lanthanide Single-Molecule Magnets. *Chem. Rev.* **2013**, *113*, 5110–5148. [CrossRef] [PubMed]

7. Zhang, P.; Guo, Y.N.; Tang, J. Recent advances in dysprosium-based single molecule magnets: Structural overview and synthetic strategies. *Coord. Chem. Rev.* **2013**, *257*, 1728–1763. [CrossRef]
8. Habib, F.; Murugesu, M. Lessons learned from dinuclear lanthanide nano-magnets. *Chem. Soc. Rev.* **2013**, *42*, 3278–3288. [CrossRef] [PubMed]
9. Goswami, S.; Mondal, A.K.; Konar, S. Nanoscopic molecular magnets. *Inorg. Chem. Front.* **2015**, *2*, 687–712. [CrossRef]
10. Osa, S.; Kido, T.; Matsumoto, N.; Re, N.; Pochaba, A.; Mrozinski, J. A Tetranuclear 3d−4f Single Molecule Magnet: $[Cu^{II}LTb^{III}(hfac)_2]_2$. *J. Am. Chem. Soc.* **2004**, *126*, 420–421. [CrossRef] [PubMed]
11. Benelli, C.; Gatteschi, D. Magnetism of Lanthanides in Molecular Materials with Transition-Metal Ions and Organic Radicals. *Chem. Rev.* **2002**, *102*, 2369–2388. [CrossRef] [PubMed]
12. Sessoli, R.; Powell, A.K. Strategies towards single molecule magnets based on lanthanide ions. *Coord. Chem. Rev.* **2009**, *253*, 2328–2341. [CrossRef]
13. Ishikawa, N.; Sugita, M.; Ishikawa, T.; Koshihara, S.-Y.; Kaizu, Y. Lanthanide Double-Decker Complexes Functioning as Magnets at the Single-Molecular Level. *J. Am. Chem. Soc.* **2003**, *125*, 8694–8695. [CrossRef] [PubMed]
14. AlDamen, M.A.; Clemente-Juan, J.M.; Coronado, E.; Martí-Gastaldo, C.; Gaita-Ariño, A. Mononuclear Lanthanide Single-Molecule Magnets Based on Polyoxometalates. *J. Am. Chem. Soc.* **2008**, *130*, 8874–8875. [CrossRef] [PubMed]
15. Zhang, P.; Zhang, L.; Lin, S.Y.; Xue, S.F.; Tang, J.K. Modulating Magnetic Dynamics of Dy_2 System through the Coordination Geometry and Magnetic Interaction. *Inorg. Chem.* **2013**, *52*, 4587–4592. [CrossRef] [PubMed]
16. Rajeshkumar, T.; Rajaraman, G. Is a radical bridge a route to strong exchange interactions in lanthanide complexes? A computational examination. *Chem. Commun.* **2012**, *48*, 7856–7858. [CrossRef] [PubMed]
17. Cucinotta, G.; Perfetti, M.; Luzon, J.; Etienne, M.; Car, P.E.; Caneschi, A.; Calvez, G.; Bernot, K.; Sessoli, R. Magnetic Anisotropy in a Dysprosium/DOTA Single-Molecule Magnet: Beyond Simple Magneto-Structural Correlations. *Angew. Chem. Int. Ed.* **2012**, *51*, 1606–1610. [CrossRef] [PubMed]
18. Ishikawa, N.; Sugita, M.; Wernsdorfer, W. Quantum Tunneling of Magnetization in Lanthanide Single-Molecule Magnets: Bis(phthalocyaninato)terbium and Bis(phthalocyaninato)dysprosium Anions. *Angew. Chem. Int. Ed.* **2005**, *44*, 2931–2935. [CrossRef] [PubMed]
19. Campbell, V.E.; Guillot, R.; Rivière, E.; Brun, P.-T.; Wernsdorfer, W.; Mallah, T. Subcomponent Self-Assembly of Rare-Earth Single-Molecule Magnets. *Inorg. Chem.* **2013**, *52*, 5194–5200. [CrossRef] [PubMed]
20. Feltham, H.L.C.; Clérac, R.; Ungur, L.; Chibotaru, L.F.; Powell, A.K.; Brooker, S. By Design: A Macrocyclic 3d–4f Single-Molecule Magnet with Quantifiable Zero-Field Slow Relaxation of Magnetization. *Inorg. Chem.* **2013**, *52*, 3236–3240. [CrossRef] [PubMed]
21. Habib, F.; Brunet, G.; Vieru, V.; Korobkov, I.; Chibotaru, L.F.; Murugesu, M. Significant Enhancement of Energy Barriers in Dinuclear Dysprosium Single-Molecule Magnets through Electron-Withdrawing Effects. *J. Am. Chem. Soc.* **2013**, *135*, 13242–13245. [CrossRef] [PubMed]
22. Tanaka, D.; Inose, T.; Tanaka, H.; Lee, S.; Ishikawa, N.; Ogawa, T. Proton-induced switching of the single molecule magnetic properties of a porphyrin based Tb^{III} double-decker complex. *Chem. Commun.* **2012**, *48*, 7796–7798. [CrossRef] [PubMed]
23. Ganivet, C.R.; Ballesteros, B.; Torre, G.; Clemente-Juan, J.M.; Coronado, E.; Torres, T. Influence of Peripheral Substitution on the Magnetic Behavior of Single-Ion Magnets Based on Homo- and Heteroleptic Tb^{III} Bis(phthalocyaninate). *Chem. Eur. J.* **2013**, *19*, 1457–1465. [CrossRef] [PubMed]
24. Langley, S.K.; Le, C.; Ungur, L.; Moubaraki, B.; Abrahams, B.F.; Chibotaru, L.F.; Murray, K.S. Heterometallic 3d−4f Single-Molecule Magnets: Ligand and Metal Ion Influences on the Magnetic Relaxation. *Inorg. Chem.* **2015**, *54*, 3631–3642. [CrossRef] [PubMed]
25. Shang, H.; Zeng, S.; Wang, H.; Dou, J.; Jiang, J. Peripheral Substitution: An Easy Way to Tuning the Magnetic Behavior of Tetrakis(phthalocyaninato) Dysprosium(III) SMMs. *Sci. Rep.* **2015**, *5*, 8838–8842. [CrossRef] [PubMed]
26. Pedersen, K.S.; Ungur, L.; Sigrist, M.; Sundt, A.; Magnussen, M.; Vieru, V.; Mutka, H.; Rols, S.; Weihe, H.; Waldmann, O.; et al. Modifying the properties of 4f single-ion magnets by peripheral ligand functionalization. *Chem. Sci.* **2014**, *5*, 1650–1660. [CrossRef]

27. Batchelor, L.J.; Cimatti, I.; Guillot, R.; Tuna, F.; Wernsdorfer, W.; Ungur, L.; Chibotaru, L.F.; Campbell, V.E.; Mallah, T. Chemical tuning of the magnetic relaxation in dysprosium(III) mononuclear complexes. *Dalton Trans.* **2014**, *43*, 12146–12149. [CrossRef] [PubMed]
28. Lin, P.-H.; Burchell, T.J.; Clérac, R.; Murugesu, M. Dinuclear Dysprosium(III) Single-Molecule Magnets with a Large Anisotropic Barrier. *Angew. Chem. Int. Ed.* **2008**, *47*, 8848–8851. [CrossRef] [PubMed]
29. Alvarez, S.; Alemany, P.; Casanova, D.; Cirera, J.; Llunell, M.; Avnir, D. Shape maps and polyhedral interconversion paths in transition metal chemistry. *Coord. Chem. Rev.* **2005**, *249*, 1693–1708. [CrossRef]
30. Kahn, M.L.; Sutter, J.-P.; Golhen, S.; Guionneau, P.; Ouahab, L.; Kahn, O.; Chasseau, D. Systematic Investigation of the Nature of The Coupling between a Ln(III) Ion (Ln = Ce(III) to Dy(III)) and Its Aminoxyl Radical Ligands. Structural and Magnetic Characteristics of a Series of {Ln(organic radical)$_2$} Compounds and the Related {Ln(Nitrone)$_2$} Derivatives. *J. Am. Chem. Soc.* **2000**, *122*, 3413–3421. [CrossRef]
31. Cole, K.S.; Cole, R.H. Dispersion and Absorption in Dielectrics I. Alternating Current Characteristics. *J. Chem. Phys.* **1941**, *9*, 341–351. [CrossRef]
32. Guo, Y.-N.; Xu, G.-F.; Guo, Y.; Tang, J. Relaxation dynamics of dysprosium(III) single molecule magnets. *Dalton Trans.* **2011**, *40*, 9953–9963. [CrossRef] [PubMed]
33. Xue, S.; Guo, Y.N.; Zhao, L.; Zhang, P.; Tang, J. Unique Y-shaped lanthanide aggregates and single-molecule magnet behaviour for the Dy4 analogue. *Dalton Trans.* **2014**, *43*, 1564–1570. [CrossRef] [PubMed]
34. Mondal, A.K.; Khatua, S.; Tomar, K.; Konar, S. Field-Induced Single-Ion-Magnetic Behavior of Octahedral Co^{II} in a Two-Dimensional Coordination Polymer. *Eur. J. Inorg. Chem.* **2016**, 3545–3552. [CrossRef]
35. Mondal, A.K.; Parmar, V.S.; Biswas, S.; Konar, S. Tetrahedral M^{II} based binuclear double-stranded helicates: Single-ion-magnet and fluorescence behaviour. *Dalton Trans.* **2016**, *45*, 4548–4557. [CrossRef] [PubMed]
36. Bartolome, J.; Filoti, G.; Kuncser, V.; Schinteie, G.; Mereacre, V.; Anson, C.E.; Powell, A.K.; Prodius, D.; Turta, C. Magnetostructural correlations in the tetranuclear series of {Fe_3LnO_2} butterfly core clusters: Magnetic and Mössbauer spectroscopic study. *Phys. Rev. B Condens. Matter Mater. Phys.* **2009**, *80*, 014430–014446. [CrossRef]
37. Lin, P.H.; Burchell, T.J.; Ungur, L.; Chibotaru, L.F.; Wernsdorfer, W.; Murugesu, M. A Polynuclear Lanthanide Single-Molecule Magnet with a Record Anisotropic Barrier. *Angew. Chem. Int. Ed.* **2009**, *48*, 9489–9492. [CrossRef] [PubMed]
38. Gamer, M.T.; Lan, Y.; Roesky, P.W.; Powell, A.K.; Clerac, R. Pentanuclear Dysprosium Hydroxy Cluster Showing Single-Molecule-Magnet Behavior. *Inorg. Chem.* **2008**, *47*, 6581–6583. [CrossRef] [PubMed]
39. Xu, G.F.; Wang, Q.L.; Gamez, P.; Ma, Y.; Clerac, R.; Tang, J.; Yan, S.P.; Cheng, P.; Liao, D.Z. A promising new route towards single-molecule magnets based on the oxalate ligand. *Chem. Commun.* **2010**, *46*, 1506–1508. [CrossRef] [PubMed]
40. Ungur, L.; Thewissen, M.; Costes, J.-P.; Wernsdorfer, W.; Chibotaru, L.F. Interplay of Strongly Anisotropic Metal Ions in Magnetic Blocking of Complexes. *Inorg. Chem.* **2013**, *52*, 6328–6337. [CrossRef] [PubMed]
41. Rinehart, J.D.; Long, J.R. Exploiting single-ion anisotropy in the design of f-element single-molecule magnets. *Chem. Sci.* **2011**, *2*, 2078–2085. [CrossRef]
42. Mondal, A.K.; Jena, H.S.; Malviya, A.; Konar, S. Lanthanide-Directed Fabrication of Four Tetranuclear Quadruple Stranded Helicates Showing Magnetic Refrigeration and Slow Magnetic Relaxation. *Inorg. Chem.* **2016**, *55*, 5237–5244. [CrossRef] [PubMed]
43. Lin, P.-H.; Sun, W.-B.; Yu, M.-F.; Li, G.-M.; Yan, P.-F.; Murugesu, M. An unsymmetrical coordination environment leading to two slow relaxation modes in a Dy_2 single-molecule magnet. *Chem. Commun.* **2011**, *47*, 10993–10995. [CrossRef] [PubMed]
44. Long, J.; Habib, F.; Lin, P.H.; Korobkov, I.; Enright, G.; Ungur, L.; Wernsdorfer, W.; Chibotaru, L.F.; Murugesu, M. Single-Molecule Magnet Behavior for an Antiferromagnetically Superexchange-Coupled Dinuclear Dysprosium(III) Complex. *J. Am. Chem. Soc.* **2011**, *133*, 5319–5328. [CrossRef] [PubMed]
45. Mondal, A.K.; Goswami, S.; Konar, S. Influence of the coordination environment on slow magnetic relaxation and photoluminescence behavior in two mononuclear dysprosium(III) based single molecule magnets. *Dalton Trans.* **2015**, *44*, 5086–5094. [CrossRef] [PubMed]
46. Rinehart, J.D.; Fang, M.; Evans, W.J.; Long, J.R. Strong exchange and magnetic blocking in N_2^{3-}-radical-bridged lanthanide complexes. *Nat. Chem.* **2011**, *3*, 538–542. [CrossRef] [PubMed]

47. Tang, J.; Hewitt, I.; Madhu, N.T.; Chastanet, G.; Wernsdorfer, W.; Anson, C.E.; Benelli, C.; Sessoli, R.; Powell, A.K. Dysprosium Triangles Showing Single-Molecule Magnet Behavior of Thermally Excited Spin States. *Angew. Chem. Int. Ed.* **2006**, *45*, 1729–1733. [CrossRef] [PubMed]
48. Kahn, O. *Molecular Magnetism*; VCH Publishers: Weinheim, Germany, 1993.
49. Naskar, S.; Mishra, D.; Chattopadhyay, S.K.; Corbella, M.; Blake, A.J. Versatility of 2,6-diacetylpyridine (dap) hydrazones in stabilizing uncommon coordination geometries of Mn(II): Synthesis, spectroscopic, magnetic and structural characterization. *Dalton Trans.* **2005**, 2428–2435. [CrossRef] [PubMed]
50. Sheldrick, G.M. *SHELXTL Program for the Solution of Crystal of Structures*; University of Göttingen: Göttingen, Germany, 1993.
51. Sheldrick, G.M. *SHELXL 97, Program for Crystal Structure Refinement*; University of Göttingen: Göttingen, Germany, 1997.
52. Spek, A.L. Single-crystal structure validation with the program PLATON. *J. Appl. Crystallogr.* **2003**, *36*, 7–13. [CrossRef]
53. Farrugia, L.J. WinGX suite for small-molecule single-crystal crystallography. *J. Appl. Crystallogr.* **1999**, *32*, 837–838. [CrossRef]